Title
In vivo Imaging of Oral Mucositis in an Animal Model Using Optical Coherence Tomography and Optical Doppler Tomography

Journal
Clinical Cancer Research, 13(8)

ISSN
1078-0432

Authors
Wilder-Smith, Petra
Hammer-Wilson, Marie J
Zhang, Jun
et al.

Publication Date
2007-04-15

DOI
10.1158/1078-0432.ccr-06-2234

In vivo Imaging of Oral Mucositis in an Animal Model Using Optical Coherence Tomography and Optical Doppler Tomography

Petra Wilder-Smith,[1] Marie J. Hammer-Wilson,[1] Jun Zhang,[1] Qiang Wang,[1] Kathryn Osann,[2] Zhongping Chen,[1] Harvey Wigdor,[3] Joel Schwartz,[3] and Joel Epstein[3]

Abstract

Purpose: To assess noninvasive optical coherence tomography (OCT) and optical Doppler tomography (ODT) for early detection and evaluation of chemotherapy-induced oral mucositis.

Experimental Design: Cheek pouches of 10 Syrian golden hamsters were imaged using OCT/ODT during development of chemotherapy-induced mucositis. I.p. injections of 5-fluorouracil and mechanical irritation induced oral lesions. At 2, 4, 7, and 11 days, one hamster was sacrificed and processed for histopathology. OCT images were visually examined; ODT results were semiquantified. Imaging data were compared with histologic findings.

Results: During the development of mucositis, OCT/ODT identified the following events: (*a*) change in epithelial thickness (beginning on day 2), (*b*) loss of surface keratinized layer continuity (beginning on day 4), (*c*) loss of epithelial (day 4 onwards) and submucosal integrity (day 7 onwards), (*d*) changes in axial blood flow velocity (increased on days 2 and 4; decreased on day 7), and (*e*) changes in blood vessel size (diameter doubled on day 2; quadrupled on day 4; unchanged on day 7). The semiquantitative imaging-based scoring system identified the severity of mucositis as defined by histopathology. The combination of imaging criteria used allowed for the detection of early, intermediate, and late mucositic changes. Imaging data gave higher scores compared with clinical scores early on, suggesting that the imaging-based diagnostic scoring was more sensitive to early mucositic change than the clinical scoring system. Once mucositis was established, imaging and clinical scores converged.

Conclusion: OCT/ODT identified chemotherapy-induced oral changes before their clinical manifestation, and the proposed scoring system for oral mucositis was validated for the semiquantification of mucositic change.

Oropharyngeal mucositis is the most common distressing and disabling acute complication of cancer chemotherapy (1) and radiotherapy (2) as reported by patients and is among the most significant major dose-limiting toxicities of cancer therapy (3, 4). Clinically, oropharyngeal mucositis (4) is characterized by mucosal changes, including erythema and ulceration, and causes oropharyngeal pain. Oropharyngeal mucositis may lead to alteration in cancer therapy, dose reduction, and delay in scheduled therapy and to interruption or termination of planned therapy, which may affect cure. In addition, oropharyngeal mucositis is associated with negative effect on quality of life and increases cost of care (5–8). Oropharyngeal mucositis is caused by several cancer treatments, including many treatments for head and neck cancer and for epithelial cancers at other body sites (e.g., gastrointestinal tract and lung), and is common in intensive chemotherapy with or without total body irradiation associated with neutropenia and hemopoietic cell transplantation. Currently, prediction of onset and severity of mucositic change is not possible, hampering efforts at targeted intervention and optimizing treatment effectiveness. The inability to characterize and measure mucositis accurately has prevented accurate evaluation of lesions and treatments. Our developing understanding of the pathogenesis of mucositis has led to increased study of preventive and treatment strategies and mucosal repair.

The occurrence of oropharyngeal mucositis can range from 30% to 75% in chemotherapy patients, up to 90% in patients receiving hemopoietic cell transplantation, and essentially in all patients receiving head and neck radiation in doses more than 5,000 cGy. Ulcerative mucositis is the most common cause of severe pain in hemopoietic cell transplantation and treatments for hematologic cancer. Whereas advances in hemopoietic cell transplantation have led to a modest reduction in the frequency of severe oral ulcerative mucositis, changes in treatment of head and neck cancer, including combined chemotherapy and irradiation, and changes in radiation therapy dosing schedules have increased the severity and duration of mucositis in these

Authors' Affiliations: [1]Beckman Laser Institute, University of California at Irvine; [2]University of California at Irvine, Irvine, California; and [3]College of Dentistry and Cancer Center, College of Medicine, University of Illinois at Chicago, Chicago, Illinois
Received 9/12/06; revised 12/5/06; accepted 1/4/07.

Grant support: Tobacco-Related Disease Research Program grant 14IT-0097 (P. Wilder-Smith, M.J. Hammer-Wilson, J. Zhang, and K. Osann); NIH Laser Microbeam and Medical Program grant P41 RR01192 (P. Wilder-Smith, M.J. Hammer-Wilson, J. Zhang, Q. Wang, K. Osann, and Z. Chen); and NIH grants EB-00255, CA-91717, and RR-01192 (Z. Chen).

The costs of publication of this article were defrayed in part by the payment of page charges. This article must therefore be hereby marked *advertisement* in accordance with 18 U.S.C. Section 1734 solely to indicate this fact.

Requests for reprints: Petra Wilder-Smith, Beckman Laser Institute, University of California at Irvine, 1002 Health Sciences Road East, Irvine, CA 92612. Phone: 949-824-7632; Fax: 949-824-8413; E-mail: pwsmith@uci.edu.

doi:10.1158/1078-0432.CCR-06-2234

Table 1. Evaluation of OCT/ODT data

OCT (structural)	OCT/ODT (vascular)
Epithelial thickness:	Blood flow velocity:
Score 0: same as day 0 (±20%)	Score 0: same as day 0 (±20%)
Score 1: reduced versus day 0 by <50%	Score 1: increased versus day 0 by >100%
Score 2: reduced versus day 0 by 50-99%	Score 2: reduced versus day 0 by >100%
Score 3: reduced versus day 0 by ≥100%	Blood vessel size:*
Loss of surface integrity:	Score 0: same as day 0 (±20%)
Score 1 if yes	Score 1: increased versus day 0 by <100%
Loss of subsurface integrity:	Score 2: increased versus day 0 by >100%
Score 2 if yes	

NOTE: Total scoring range for OCT (structural) lies between 0 and 6. Total scoring range for OCT plus ODT (vascular) lies between 0 and 4.

*ODT scale based on vascular effects previously described in mild and severe mucositis, not on progressive change in blood flow (5, 35, 36).

patients (9). A recent article reports the successful imaging of mucositic changes in the rat model (10).

Optical Coherence Tomography and Optical Doppler Tomography

Optical coherence tomography (OCT) is a high-resolution optical technique that permits minimally invasive imaging of near-surface abnormalities in complex tissues. Conceptually, it has been compared with ultrasound scanning (11). Both ultrasound and OCT provide real-time structural imaging, but unlike ultrasound, OCT is based on low-coherence interferometry using broadband light to provide cross-sectional, high-resolution subsurface tissue images (12–17). Broadband laser light waves are emitted from a source and directed toward a beam splitter; one wave is sent toward a reference mirror with known path length and the other toward the tissue sample. After the two beams reflect off the reference mirror and tissue sample surfaces at varying depths within the sample, the reflected light is directed back toward the beam splitter, where the waves are recombined and read with a photo detector. The image is produced by analyzing interference of the recombined light waves. Cross-sectional images of tissues are constructed in real time at near histologic resolution (~10 μm with current technology). This permits *in vivo* noninvasive imaging of the microscopic characteristics of epithelial and subepithelial structures, including (*a*) depth and thickness, (*b*) histopathologic appearance, and (*c*) peripheral margins. With a tissue penetration depth of 1 to 2 mm, the imaging range of the OCT technology described in this article is suitable for imaging of the oral mucosa (18–21). Previous studies using OCT have shown the ability to evaluate characteristics of epithelial, subepithelial, and basement membrane structures and show the potential for near histopathologic level resolution and close correlation with histologic appearance (18, 21–27).

Optical Doppler tomography (ODT) combines Doppler velocimetry with OCT, resulting in extremely high-resolution tomographic images of static and moving constituents in highly scattering biological tissues (28–30). Based on a phase-resolved technique (28, 31), high spatial resolution and high-velocity sensitivity can be obtained simultaneously without compromising the image speed. Because images of blood vessels, blood flow, and tissue structure are obtained simultaneously from a single scan, OCT/ODT has decided advantages over existing methodologies for investigating vascularization and altered tissue perfusion and epithelial and subepithelial change.

As changes in epithelial architecture, blood vessel size, and blood flow can be imaged and quantified accurately using OCT/ODT (18, 25, 28), early detection and tracking of these changes by OCT/ODT should be successful. These changes, also, are amenable to imaging and quantification using OCT/ODT (18, 25, 28). Mucosal thinning and vascular change are clearly visible and measurable in OCT/ODT images (18, 25, 28). In this feasibility study, the ability of OCT/ODT to detect and characterize chemotherapy-induced oral mucositis was evaluated.

Materials and Methods

Animal model. I.p. injections of 5-fluorouracil on days 0, 5, and 10 (60 mg/kg) and mechanical cheek pouch irritation were used to induce mucositis in the right cheek pouches of 10 young Syrian golden hamsters as described previously (32). This model has been shown to mimic ulcerative oral mucositis in humans. One week before this process, after baseline OCT/ODT imaging, two sutures were placed in each cheek pouch as markers for the accurate relocalization of subsequent imaging scans. This process was done 1 week before the experimental protocol to minimize the effects of suture placement on protocol data. At days 2, 4, 7, and 11, a hamster was sacrificed and the treated cheek pouch was processed for 3-μm serial sectioning, H&E staining, and histopathologic evaluation. During the study period, animals were examined daily for general appearance and mucositis evaluation. The animals were photographed and then imaged on days 0, 2, 4, 7, and 11 by OCT/ODT using a 6-mm scan line with marker sutures as scan line end points. All procedures were carried out in compliance with University of California at Irvine Institutional Animal Care and Use Committee guidelines under protocol 97-1972.

OCT and ODT imaging and histology. A broadband light source from a 1,310-nm superluminescent diode with a FWHM bandwidth of 75 nm was used as the light source for the OCT/ODT system. The light was split into reference and sample arms by a 2 × 2 coupler. In the reference arm, a rapid scanning optical delay line was used to provide

Table 2. Modified Oral Mucositis Assessment Scale for oral mucositis in the hamster cheek pouch model

Area of ulceration*	Severity of erythema†		
0	0	1	2
1	1	2	3
2	2	3	4
3	3	4	5

*Area of ulceration: 0 = none; 1 = <4 mm^2; 2 = 4-9 mm^2; 3 = >9 mm^2.

†Severity of erythema: 0 = none; 1 = not severe; 2 = severe.

group delay without phase modulation (33, 34). A stable carrier frequency was generated by an electro-optical phase modulator for heterodyne detection. A probe with a collimator and an objective lens driven by a translation stage were used in the sample arm. Doppler processing was implemented from the phase term to visualize blood flow. The Doppler frequency shift and the SD of the Doppler frequency spectrum were calculated from the average phase shift between sequential A scans to determine velocity vector of the blood flow. A visible aiming beam (633 nm) was used to find and locate the exact imaging position on the sample.

The phase-resolved OCT/ODT system used in these studies had the following performance variables: (*a*) axial resolution, 10 μm; (*b*) axial scan frequency, 1 to 4 kHz; (*c*) frame rate, 1 to 8 frame/second; (*d*) imaging depth, 1 to 2 mm; and (*e*) velocity sensitivity, 10 μm/s. Imaging was done *in vivo* using a 6-mm scan line with the marker sutures as scan line end points. Acquisition time for each image was <1 s. For imaging, the animals were anesthetized using 200 mg/kg i.p. ketamine and 10 mg/kg i.p. xylazine. They were wrapped in a Mylar blanket to prevent hypothermia and monitored closely throughout imaging. After imaging and recovery from anesthesia, the animals were returned to their cages. Hamsters were sacrificed using lethal i.c. injection of sodium pentobarbitol. Oral tissues were immediately excised and processed for histopathology. Serial sections (3 μm) were prepared from the area of OCT imaging and stained with H&E before microscopic analysis. Histopathology was assessed by one blinded observer.

Evaluation of OCT/ODT data. Two prestandardized scorers classified each image diagnostically in a blind manner on the scale of 0 to 10 described below. Scorers (one oral pathologist and one dentist, both with >1 year of experience in evaluating oral OCT and ODT images) were pretrained using a standard set of 50 OCT/ODT and 50 matching histopathologic images of oral mucositis. Initial training was repeated until at least 96% of images were identified correctly, and then, 50 new sets of OCT/ODT and histopathology images were identified by each scorer with at least 90% accuracy. At this stage, scorers were deemed "prestandardized" and ready to participate in these studies. Each scorer evaluated all data in one session, which took place once all data accrual was complete. Imaging (OCT and ODT) diagnostic scores were defined as described in Table 1.

Increased blood flow velocity was assigned a score of +1 and decreased blood flow velocity was assigned a score of +2 because ODT data confirmed the observation described in several articles (5, 35, 36) that, during mucositis development, initial early increases in blood flow are followed by engorgement and stagnation during later, clinically more severe mucositis. The proposed ODT scoring scale is based on the premise that an increasing score reflects an increasing severity of the mucositis rather than a progressive increase in blood flow.

Combining the scores from OCT (structural) with those from OCT/ODT (vascular), the cumulative scoring scale for mucositic severity ranged from 0 to 10.

Results

Gross observations

Day 2. No clinical changes were evident.

Day 4. Mucosal erythema was clinically evident in all animals. Microabscess were present in 2 of 10 animals.

Day 7. Frank localized ulceration and epithelial breakdown were visible in all animals.

Day 11. Marked epithelial disruption, surface necrosis, and mucosal breakdown were seen in all animals.

For the semiquantification of clinical changes, a cumulative scoring system in a scale of 0 to 5 based on the Oral Mucositis Assessment Scale was used (Table 2). The category "area of ulceration" was modified from the original scale for humans to compensate for the smaller size of the hamster cheek pouch.

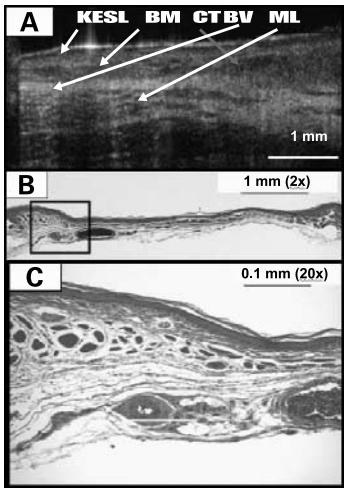

Fig. 1. *A* to *C,* noninvasive *in vivo* OCT image and H&E-stained sections of healthy hamster cheek pouch before the commencement of mucositis induction. In the OCT image, the keratinized epithelial surface layer (*KESL*), basement membrane (*BM*), underlying connective tissues (*CT*) and blood vessels (*BV*), as well as muscle layer (*ML*) are clearly visible. Corresponding structures are seen in the stained tissue section in (*B*) and (*C*).

Microscopic features

Days 2 to 4. Parakeratosis and hydropic degeneration became evident. Localized infiltrations of polymorphonuclear leukocytes were observed. Lymphocyte and macrophage infiltration was evident in and around the dilated capillaries of the connective tissues. The capillaries in the connective tissues were dilated and engorged with erythrocytes (Figs. 1–4).

Days 7 to 11. Considerable epithelial destruction related to severe ulceration was common. Large zones of hydropic degeneration and parakeratosis were observed. Patches of fibrin deposition were evident. The connective tissues also showed large areas of destruction associated with tissue sloughing and infection. Extensive collagen degeneration was seen. In the many dilated and engorged capillaries, an extensive mixed inflammatory exudate was common.

Imaging data

Using imaging, the following events were detected: (*a*) change in epithelial thickness (day 2 onwards), (*b*) loss of surface keratinized layer continuity (day 4 onwards), (*c*) loss of epithelial (day 4 onwards) and submucosal integrity (day 7 onwards), (*d*) changes in axial blood flow velocity versus day 0 (increased on day 2 and 4; decreased on day 7), and (*e*) changes in blood vessel size versus day 0 (diameter doubled on day 2; quadrupled on day 4; unchanged on day 7; Figs. 1–4).

Analysis of semiquantified imaging data

Comparison of imaging scores versus clinical mucositis scores (Oral Mucositis Assessment Scale). Figure 5 shows the total imaging score (and SE) during the development of mucositis. For the total imaging score, differences between each pair of successive time points were significant, with $P < 0.0005$ using the Kruskal-Wallis nonparametric test, which is appropriate given the small numbers. This means that the imaging scoring approach was capable of mapping accurately and effectively the severity of the mucositic condition. The imaging data tended to give higher scores compared with clinical scores early on

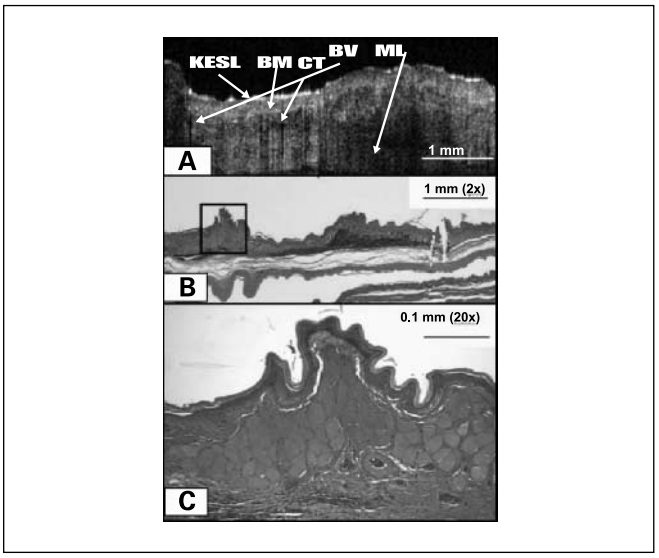

Fig. 2. *A* to *C,* noninvasive *in vivo* OCT image and H&E-stained sections of hamster cheek pouch 4 d after the commencement of mucositis induction. In the OCT image, the keratinized epithelial surface layer is mildly reduced in thickness and the basement membrane, underlying connective tissues and blood vessels, as well as muscle layer are clearly visible. The blood vessel is dilated. Corresponding structures are seen in the stained tissue section in (*B*) and (*C*): the epithelium is somewhat thinner and an infiltration of lymphocytes and macrophages is noted, with a tendency to perivascular distribution. Localized polymorphonuclear leukocyte infiltrations are seen.

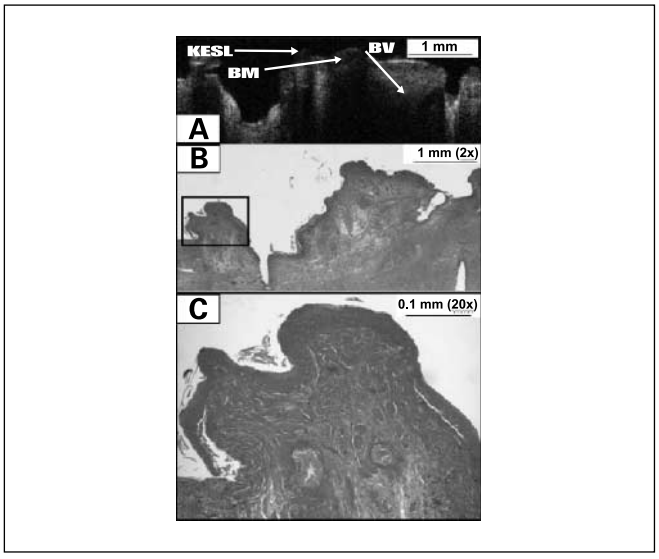

Fig. 4. *A* to *C,* noninvasive *in vivo* OCT image and H&E-stained sections of hamster cheek pouch after 11 d of mucositis induction. In the OCT image, the epithelium is only present in small patches and the keratinized epithelial surface layer is almost completely lost. The tissues appear swollen and indistinct with extensive areas of tissue degeneration. A blood vessel is visible, which appears partly collapsed. In the stained tissue section in (*B*) and (*C*), considerable epithelial destruction is apparent and the surface keratinized layer is mostly lost. Areas of liquefaction degeneration and collagen degeneration are visible, and an infiltration of lymphocytes, polymorphonuclear leukocytes, and macrophages is noted.

(days 0-4; see Fig. 5). However, correspondence was good at days 7 and 11 (nonsignificant Wilcoxon rank-sum test and moderate Spearman and Pearson correlation coefficients). These data indicate that the imaging-based diagnostic scoring was more sensitive to early mucositic change than the clinical scoring system. Once mucositis was established and the clinical manifestation of the condition was more advanced, the imaging and clinical scores converged. Clinically, this finding was highly relevant, as earlier detection of mucositic change will allow the earlier and more effective instigation of antimucositic measures.

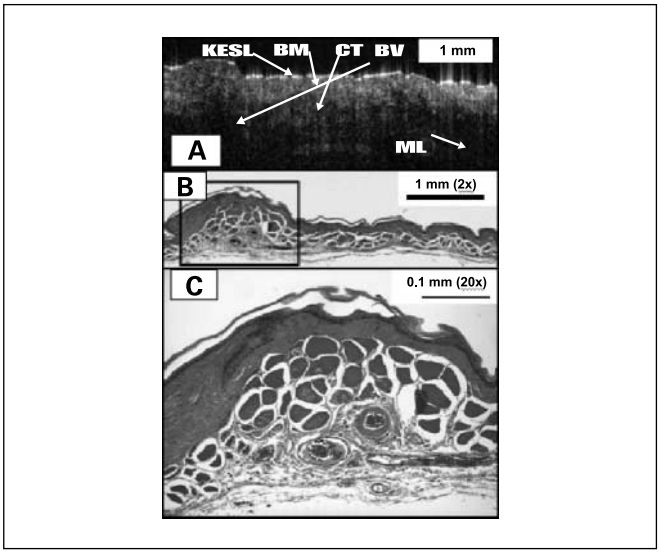

Fig. 3. *A* to *C,* noninvasive *in vivo* OCT image and H&E-stained sections of hamster cheek pouch after 7 d of mucositis induction. In the OCT image, the keratinized epithelial surface layer is markedly reduced in thickness and patches of the keratinized surface layer have been lost. The basement membrane has become convoluted, and the tissues appear swollen and indistinct with areas of liquefaction degeneration. An engorged blood vessel is visible. In the stained tissue section in (*B*) and (*C*), the epithelium is markedly thinner, with areas of parakeratosis and detachment of the surface keratinized layer. Areas of liquefaction degeneration and collagen degeneration are visible, and an infiltration of lymphocytes, polymorphonuclear leukocytes, and macrophages is noted, with a tendency to perivascular distribution. Dilated and engorged blood vessels are seen.

Analysis of imaging scoring criteria. Figure 6 shows mean scores (and SE) for each of the imaging scoring criteria over days 0 to 11. Using the Kruskal-Wallis nonparametric test (appropriate given the small numbers), there was a significant change in score over time for each measure ($P < 0.05$), confirming the appropriateness of the scoring criteria for measuring mucositis. The combination of criteria used allowed for the detection of early (EPTH, BFV, and BVS), intermediate (EPTH, LSI, LSSI, and BVS), and late (EPTH, LSSI, and BFV) changes in the oral mucosa related to the development of mucositis.

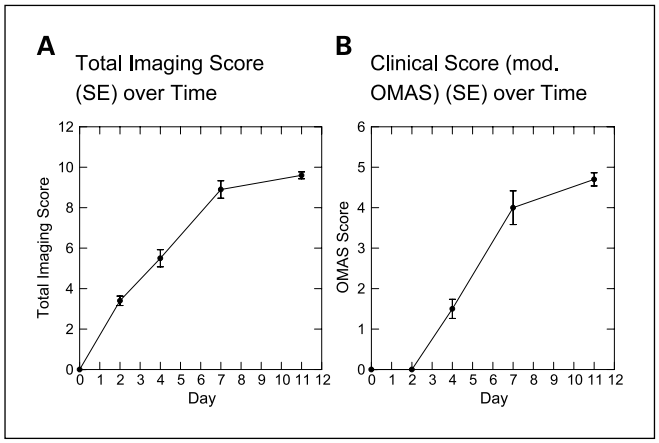

Fig. 5. *A,* total imaging score (SE) over time. *B,* clinical score [modified Oral Mucositis Assessment Scale (*OMAS*); SE] over time.

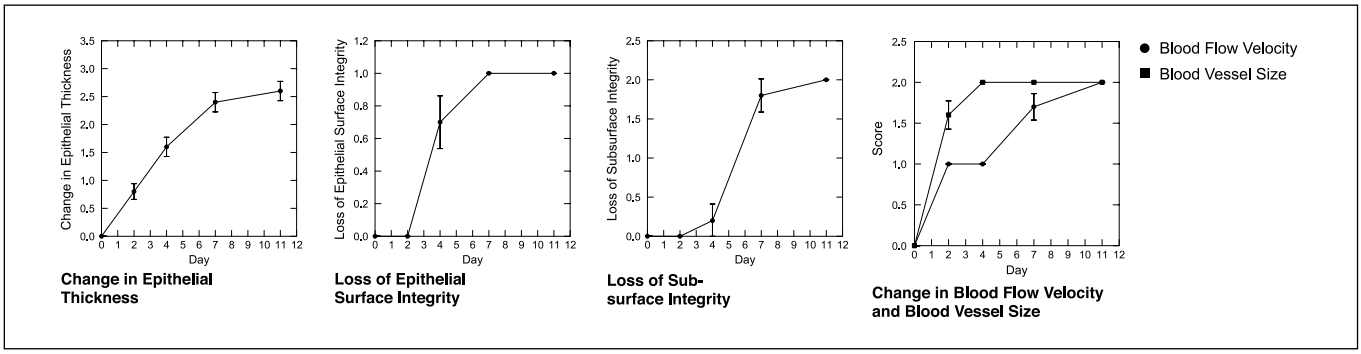

Fig. 6. Change in each imaging scoring criterion over time.

Discussion

OCT/ODT achieved noninvasive, rapid, real-time imaging of oral mucosa and identified structural and vascular changes during the development of oral mucositis. Epithelial thinning, vasodilation, and increased blood flow velocity in the epithelium and connective tissue were mapped before clinical evidence of mucositis (day 2). Further changes were evident using noninvasive imaging by the time clinical erythema was seen (day 4), including increased epithelial thinning, loss of surface integrity, and increased vasodilation, but no further change in blood flow velocity. By the time clinical ulceration developed, OCT images showed epithelial disintegration, liquefactive necrosis, and ulceration. Blood vessel size remained unchanged from the prior level of vasodilation and blood flow increased only slightly. OCT images resembled histologic findings at all time points.

The semiquantitative imaging-based scoring system effectively and accurately identified the severity of oral mucositis. The imaging data tended to give higher scores compared with clinical scores early in the course of mucosal damage, with initial changes in the vasculature and blood flow, indicating that the imaging-based diagnostic scoring is more sensitive to early mucositic change than the clinical scoring system. Clinically, this finding is highly relevant, as earlier detection of mucosal damage will allow the earlier intervention and offers the potential for prevention or reduction of severity of mucositis. In addition, OCT/ODT imaging may provide more effective investigation of preventive and therapeutic interventions for mucositis. Once mucositis was established and the clinical manifestation of the condition was more advanced, the imaging and clinical scores converged.

Although OCT/ODT technology is currently limited in its availability to clinicians, its accessibility is increasing rapidly as its costs diminish and turnkey systems can readily be purchased. Clinical and research implications of the imaging-based scoring system are considerable and include the following. (*a*) Accurate scoring of the level of mucositis will permit effective communication between treating physicians and will improve the ability to assess the severity of therapy-induced mucositis and the effectiveness of interventional measures. (*b*) The ability to quantify epithelial connective tissue and vascular change (which is currently impossible) will lead to a better understanding of the mucositic process, of patient susceptibility, and of the mechanisms and effectiveness of interventions. (*c*) Imaging-based diagnostics will permit very early identification of at risk patients, early initiation (and greater success) of the most appropriate interventions, as well as monitoring of interventional effects and effectiveness. Although not assessed in this study, it is likely that healing may be visible on OCT/ODT before clinical evidence of resolution of tissue damage. The tailoring of interventions (e.g., by using a preventive agent initially followed by a healing promoter at the appropriate time point) based on the *in vivo* imaging data is very attractive. The high cost of managing mucositis adds to the urgency for instituting imaging-based diagnostics in patients receiving cancer therapy. (*d*) The accurate mapping of the epithelial connective tissue and vascular components of mucositis will greatly enhance our understanding of the mechanisms involved in the interventions currently under investigation. For example, some interventions, such as keratinocyte growth factor (KGF), are thought to have vascular or epithelial effects.

Conclusion

In the hamster model, noninvasive OCT/ODT is capable of measuring changes in subsurface architecture and vascularity during the development of chemotherapy-induced mucositis. Correlations between OCT/ODT data and histology are clearly shown.

References

1. Epstein JB, Stevenson-Moore P, Jackson SM, Mohamed JH, Spinelli JJ. Prevention of oral mucositis in radiation therapy: a controlled study with benzydamine hydrochloride rinse. Int J Radiat Oncol Biol Phys 1989;16:1571–5.
2. Epstein JB. Infection prevention in bone marrow transplantation and radiation patients. NCI Monogr 1990;9:73–85.
3. Epstein JB, Schubert MM, Scully C. Evaluation and treatment of pain in patients with orofacial cancer: a review. Pain Clin 1991;4:3–20.
4. Epstein JB. Oral complications of cancer chemotherapy: etiology, recognition and management. Can J Oncol 1992;2:83–95.
5. Sonis ST, Elting LS, Keefe D, et al. Perspectives on cancer therapy-induced mucosal injury: pathogenesis, measurement, epidemiology, and consequences for patients. Cancer 2004;100:1995–2025.
6. Sonis ST, Oster G, Fuchs H, et al. Oral mucositis and the clinical and economic outcomes of hematopoietic stem-cell transplantation. J Clin Oncol 2001;19:2201–5.
7. Elting LS, Shih YC. The economic burden of supportive

care of cancer patients. Support Care Cancer 2004; 12:219–26.

8. Elting LS, Cooksley C, Caambers M, Cantor SBN, Manzullo F, Rubenstein EB. The burdens of cancer therapy. Clinical and economic outcomes of chemotherapy-induced mucositis. Cancer 2004;100: 1324–6.

9. Modi BJ, Knab B, Feldman LE, et al. Review of current treatment practices for carcinoma of the head and neck. Expert Opin Pharmacother 2005;6:1143–55.

10. Muanza TM, Cotrim A, McAuliffe M, et al. Evaluation of radiation-induced oral mucositis by optical coherence tomography. Clin Cancer Res 2005;11: 121–5127.

11. Tadrous PJ. Methods for imaging the structure and function of living tissues and cells. I. Optical coherence tomography. J Pathol 2000;191:115–9.

12. Izatt JA, Kulkarni MD, Kobayashi K, Sivak MV, Barton JK, Welch AJ. Optical coherence tomography for biodiagnostics. Opt Photon News 1997;8:41–7.

13. Ding Z. High-resolution optical coherence tomography over a large depth range with an axicon lens. Opt Lett 2002;27:4.

14. Huang D, Swanson EA, Lin CP, et al. Optical coherence tomography. Science 1991;254:1178–81.

15. Swanson EA, Izatt JA, Hee MR, et al. *In vivo* retinal imaging by optical coherence tomography. Opt Lett 1993;18:1864–6.

16. Fujimoto JG, Hee MR, Izatt JA, et al. Biomedical imaging using optical coherent tomography. Proc SPIE 1999;3749:402.

17. Bouma B,Tearney GJ, Boppart SA, Hee MR, Brezinski ME, Fujimoto JG. High-resolution optical coherence tomographic imaging using a mode-locked Ti:Al/sub 2/O/sub 3/laser source. Opt Lett 1995;20:1486–8.

18. Wilder-Smith P, Jung WG, Brenner M, et al. Optical coherence tomography for the diagnosis of oral malignancy. Lasers Surg Med 2004;35:269–75.

19. Matheny E, Mina-Araghy R, Hama N, et al. Optical coherence tomography of malignancy in the hamster cheek pouch. J Biomed Opt 2004;9:978–81.

20. Matheny ES, Hanna N, Mina-Araghi R, et al. Optical coherence tomography of malignant hamster cheek pouches. J Invest Med 2003;51:S78.

21. Boppart SA, Hee MR, Fumimoto JG, et al. Dynamic evolution and *in vivo* tomographic imaging of laser-induced retinal lesions by using optical coherence tomography. IEEE/Proceeding Conference on Lasers and Electro-Optics, Baltimore, MD, May 1995.

22. Milner TE, Dave D, Zhongping C, Goodman DM, Nelson JS. Optical coherence tomography as a biomedical monitor in human skin. In: Alfano RR, Fujimoto JG, editors. Optical Society of America (OSA); Washington, DC. 1996. p. 220–3.

23. Bamford KJ, James SW, Barr H, Tatam RP. Optical low coherence tomography of bronchial tissue. Proc SPIE 1999;3858:172–9.

24. Wilder-Smith P, Osann K, Hanna N, et al. *In vivo* multiphoton fluorescence imaging: a novel approach to oral malignancy. Lasers Surg Med 2004;35:96–103.

25. Wilder-Smith P, Krasieva T, Jung WG, et al. Noninvasive imaging of oral premalignancy and malignancy. J Biomed Opt 2005;10:051601-1–0501601-8.

26. Jung WG, Zhang J, Wang L, et al. Three-dimensional optical coherence tomography employing a 2-axis MEMS. IEEE J Sel Top Quant Electron 2006;11:806.

27. Jung WG, Zhang J, Chung JR, et al. Advances in oral cancer detection using optical coherence tomography. IEEE J Sel Top Quant Electron 2006;11:811.

28. Chen Z, Zhao Y, Saxer C, Xiang S, De Boer JF, Nelson JS. Phase-resolved OCT/ODT for imaging tissue microcirculation. Proc SPIE 2000;3915:413–4.

29. Chen Z, Milner TE, Wang X, Srinivas S, Nelson JS. Optical Doppler tomography: imaging *in vivo* blood flow dynamics following pharmacological intervention and photodynamic therapy. Photochem Photobiol 1998;67:56–60.

30. Perree J, van Leeuwen TG, Pasterkamp G, Izatt JA. Imaging of atherosclerotic plaques by optical coherence tomography (OCT). SPIE 2000;3915:522–7.

31. Chen Z, Milner TE, Srinivas S, et al. Noninvasive imaging of *in vivo* blood flow velocity using optical Doppler tomography. Opt Lett 1997;22:1119–21.

32. Sonis STY, Tracey C, Shklar G, Jenson J, Florine D. An animal model for mucositis induced by cancer chemotherapy. Oral Surg Oral Med Oral Pathol 1990;69: 437–43.

33. Tearney GJ, Bouma BE, Fujimoto FG. High-speed phase- and group-delay scanning with a grating-based phase control delay line. Opt Lett 1997;22: 1811–3.

34. Rollins AM, Kulkarnis MD, Yazdanfar S, Ungarunyawee R, Izatt JA. *In vivo* video rate optical coherence tomography. Opt Express 1997;3:219–29, 36.

35. Sonis ST. Oral mucositis in cancer therapy. J Support Oncol 2004;2:3–8.

36. Sonis ST. A biological approach to mucositis. J Support Oncol 2004;2:21–32; discussion 35–6.